16

Computer-Aided Assessment and Stenting of Tracheal Stenosis

Rômulo Pinho, Kurt G. Tournoy, and Jan Sijbers

CONTENTS

16.1 Introduction

Tracheal stenosis is an unnatural narrowing of the trachea with traumatic, neoplastic, or idiopathic causes that, despite being relatively rare, can be life threatening (Spittle and McCluskey, 2000). Until now, tracheal resection surgery remains the preferred choice of treatment. In this modality, the narrowed part of the trachea is removed and the ends are sutured together (Elliott et al. 2003; Grillo et al. 1995). When the stenosis is too long or when the patient status does not permit a surgical procedure, stent implants can render a successful solution to the stricture (Venuta et al. 2004; Saito and Imamura, 2005). Stents are tubular structures, currently made of silicone or metallic alloys, used to return normal breathing function to a patient by pushing the narrowed regions of the trachea. Since they are usually implanted with bronchoscopes, they reduce the surgical risk to the patient, especially when compared with tracheal resection (Ching-Yang et al. 2007; Mandour et al. 2003; Miyazawa et al. 2004).

The choice of treatment is a direct result of the assessment of the stenosis. It means that, when assessing the stenoses, it is important to correctly determine their location, length, and degree of narrowing (Boiselle et al. 2008). Traditionally, stenoses have been assessed with rigid or flexible bronchoscopy (Carretta et al. 2006; Nouraei et al. 2006). These methods, however, are invasive, often require patient sedation, and render subjective results, which depend on the expertise of the specialist in charge. Bronchoscopic methods may not even serve their purpose if the stricture is too narrow to allow the passage of the bronchoscope itself. If a stent is to be used in the treatment, the assessment also determines its dimensions (external diameter and length) and deployment location.

With advances in the imaging field, image analysis has increasingly been used as a complementary tool for the assessment of stenosis and computed tomography (CT) is often the imaging modality of choice. A variety of methods have been proposed to assess stenosis using CT image analysis and processing. Lee et al. (2005) reviewed the use of multislice CT analysis in prestenting and poststenting scenarios. Shitrit et al. (2005) and Hoppe et al. (2004) showed that virtual bronchoscopy can be used in training as well as in real cases. A precondition to a successful treatment with stents is that the size and diameter of the tubes must be correctly estimated; otherwise, problems such as stent migration and improper mucus clearance often occur (Venuta et al. 2004; Saito and Imamura, 2005; Prasad et al. 2002; Carretta et al. 2006). Further improvements to traditional assessment methods have been proposed. In many cases, the cross-sectional diameter or area profile of the trachea is extracted from the CT images and plotted on a graph (Graham et al. 2000; Sorantin et al. 2002; Kiesler et al. 2007; Triglia et al. 2002). Ballester et al. (2009) proposed a graphical user interface in which the physician manually places a stent in the CT image of the patient. Despite these improvements, tracheal stenosis assessment and stent choice remain, to date, operator-dependent operations.

This chapter describes and discusses traditional and computer-aided methods for the assessment and stenting of tracheal stenosis. In particular, a new method proposed by Pinho et al. (2010) is described in detail. This method uses deformable shape models to estimate the healthy trachea of patients (i.e., in case stenosis was not present) and segment the narrowed tracheas from their chest CT scans. Healthy and narrowed versions of the trachea are compared in order to automatically detect the stenoses and their parameters. The parameters are eventually used in the automatic suggestion of patient-specific stents.

In the remainder of the chapter, the reader is first provided with a brief clinical background on the anatomy of the trachea and the main characteristics of stenosis and stents (Section 16.2). Section 16.3 reviews traditional methods for assessment of stenosis, whereas Section 16.4 discusses computer-aided techniques. The method presented by Pinho et al. (2010) is described in Section 16.5, and the chapter is concluded in Section 16.6.

16.2 Clinical Background

16.2.1 Anatomy of the Trachea

The tracheobronchial tree constitutes the airway below the vocal cords. Consisting of a hierarchical group of tubular structures, the trachea is the primary tube of this tree. It functions as a conduit for ventilation and clearance of secretions.

The shape of the healthy trachea may present considerable variation. Changing with age, it gradually goes from funnel-shaped in infancy to ovoid in adulthood. The radial shape is normally ovoid anteroposteriorly but can also appear ovoid in the sagittal direction, be circular or, less frequently, slightly triangular. Unique and unexplained distortions may occur as well (Grillo et al. 1995). The length goes from 9 to 12 cm in adults, measured from the lower border of cricoid cartilage down to the top of the carinal spur, while the average laterolateral diameter is between 1.3 and 2.2 cm (Webb et al. 2000; Grillo et al. 1995).

The trachea is composed of 18 to 22 anteriorly located horseshoe-shaped cartilaginous open circles, whose ends are posteriorly connected by a soft membrane. It bifurcates approximately at the sternal angle into the left and right main bronchi, and the carina is the ridge separating their openings. On CT, the tracheal wall is usually visible as a 1- to 3-mm soft tissue stripe, delineated internally by air in the tracheal lumen and externally by mediastinal fat, the lungs, larger vessels, and the esophagus. The posterior tracheal wall appears thinner and more variable in contour, since it lacks cartilage. It can appear convex, concave, or flat. During expiration, CT typically shows significant anterior bulging of the posterior membrane, but the anterior and lateral walls change little (Webb et al. 2000). Figure 16.1 provides illustrations of the tracheal anatomy.

16.2.2 Tracheal Stenosis

Tracheobronchial stenosis is defined as focal or diffuse narrowing of the tracheal lumen (Figure 16.2). By far, the most common cause of tracheal stenosis is trauma, specifically internal trauma, usually occasioned by any type of intubation (Grillo, 2004; Boiselle et al. 2008; Lee and Boiselle, 2008). There are other potential causes of tracheal stenosis, including inflammatory diseases, benign or malignant neoplastic conditions, and extrinsic

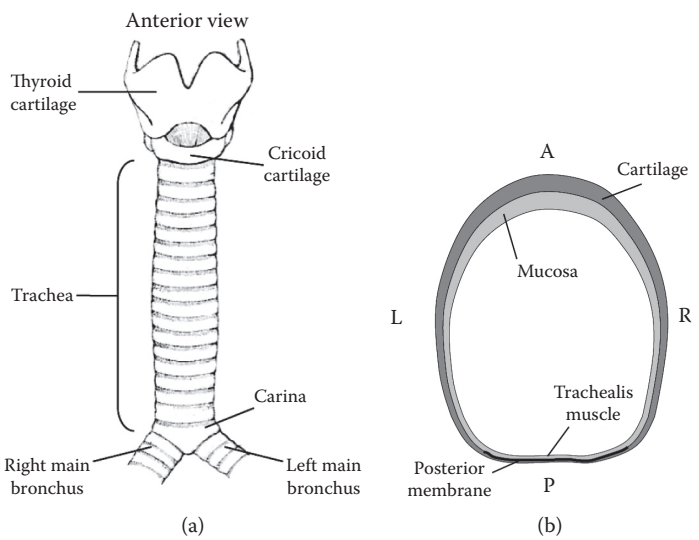

FIGURE 16.1
Different views of the trachea and its composing structures: (a) illustration of the whole trachea and (b) schematic view of an axial cross section.

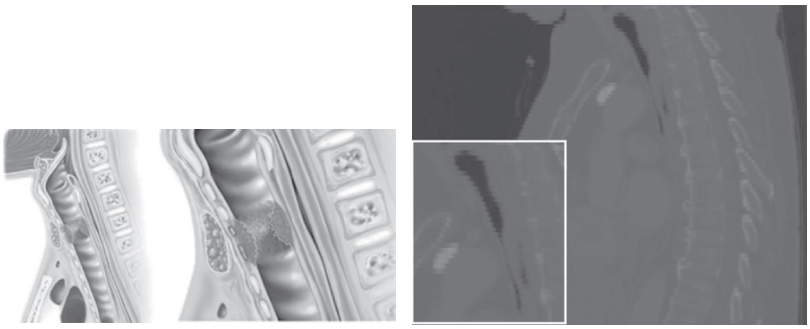

(a) (b)

FIGURE 16.2
(a) A schematic view of stenosis. (Courtesy of Dr. P. Delaere, Center for Larynx, Trachea and Hypopharynx Reconstruction, Katholieke Universiteit Leuven, Belgium.) (b) A real case showing one sagittal slice of a chest CT scan.

pressure. In addition, idiopathic narrowing of the trachea is not completely uncommon, predominantly appearing in women (Grillo et al. 1995).

Typical symptoms of tracheal stenosis include shortness of breath, coughing, and stridor. The narrowing may be seen in various different shapes. It typically extends from 1.5 to 2.5 cm in length (Webb et al. 2000), but cases of long-segment tracheal stenosis have also been reported (Elliott et al. 2003). It has also been reported that the shape of the stricture is usually associated with its causes (Lee and Boiselle, 2008; Webb et al. 2000).

16.2.3 Tracheal Stents

The medical term *stent* was introduced by Charles R. Stent, a British dentist who developed a device that supported the healing of gum grafts. The term has since been used to refer to any device designed to maintain the integrity of hollow tubular structures (Saito and Imamura, 2005; Freitag, 2000). Tracheal stents are tubular structures, currently made of silicone or metallic alloys, used to return normal breathing function to the patient by pushing the narrowed regions of the trachea (Ching-Yang et al. 2007; Mandour et al. 2003; Miyazawa et al. 2004). Examples of the different materials, shapes, and sizes of coated and uncoated stents are shown in Figure 16.3.

Although airway resection and reconstruction is most often the preferred therapy for both benign and malignant lesions, a variety of factors, including long stenosis, failed previous repair, metastatic or unresectable malignancy, or even patient refusal,may dictate nonsurgical management. In these cases, bronchoscopic treatment is indicated, and the use of stents is also an option. There are three indications for the use of stents: support of weakened tracheal walls due to tracheal malacia, re-establishment of the full tracheal lumen in case of extrinsic pressure, and sealing of fistulas toward the esophagus or pleural cavity (Freitag, 2010; Venuta et al. 2004; Saito and Imamura, 2005; Stephens and Wood, 2000; Ching-Yang et al. 2007; Mandour et al. 2003; Miyazawa et al. 2004).

Good results from airway stenting largely depend on patient selection, but satisfactory to excellent results are generally achieved in most patients undergoing airway stenting (Saito and Imamura, 2005). The tubes have also been used in tracheal reconstruction surgeries to aid the support and recovery of the reconstructed areas (Stamenkovic et al. 2007).

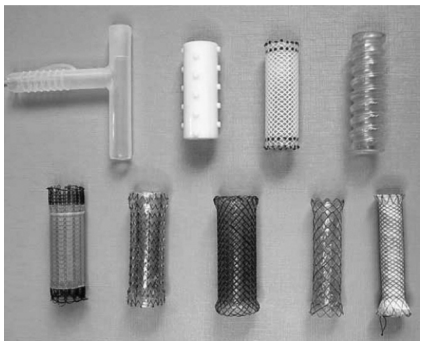

FIGURE 16.3
Typical tracheal stents. (top, left to right) Montgomery T stent, Dumon stent, Polyflex stent, and Noppen stent. (bottom, left to right) Ultraflex stent, Aero stent, Eco Nanjing stent, Hanaro stent, and Tae woong stent. (From Freitag, copyright ERS, 2010. With permission.)

In addition, stents are valuable complementary tools to other healing techniques and can provide prolonged palliation. More important, it is the only bronchoscopic technique to provide a solution for extrinsic compression (Wood et al. 2003).

The size of the stent should be adjusted according to the normal diameter proximal and distal to the area of stenosis. A narrow stent risks displacement and will be separated from the tracheal wall with failure of incorporation into the mucosa. A wider stent may lead to wall necrosis or excessive elongation with proximal or distal airway obstruction. Stents that are too long, in turn, can impede mucus clearance. Stent choice thus depends on the characteristics of the stenosis and on a physician's training and experience. Devices such as the AeroSizer® (Merit Medical Systems, South Jordan, UT) have even been created to aid in the stent sizing process. A rule of thumb is that the stent should extend 0.5 cm at each end of the stenosis (Freitag, 2010; Venuta et al. 2004; Graham et al. 2000; Ching-Yang et al. 2007; Grillo, 2004; Wood et al. 2003; Mostafa, 2003). Lee et al. (2010) reported that a stent alert card detailing the type and dimensions of the stent and its location in the tracheobronchial tree should be given to the patient. It should also indicate the appropriate size of endotracheal tube to be used if emergent intubation is required with the stent in site.

In our clinical routine, the healthy diameter of a patient's trachea is guessed from the images available. Image sources include bronchoscopy, CT, and three-dimensional (3D) reconstructions. The start and end points and the degree of narrowing of the stenosis are then visually estimated from this guess. In general, stents can be the treatment of choice for strictures with a degree of narrowing between 25% and 75%.

16.3 Traditional Methods for Airway Assessment

16.3.1 Rigid Bronchoscopy

The technique and clinical application of bronchoscopy was introduced by the German doctor Gustav Killian in 1897, when he first employed an endoscope to examine the airways. His tool was in fact an esophagoscope, which he used to remove a piece of pork bone

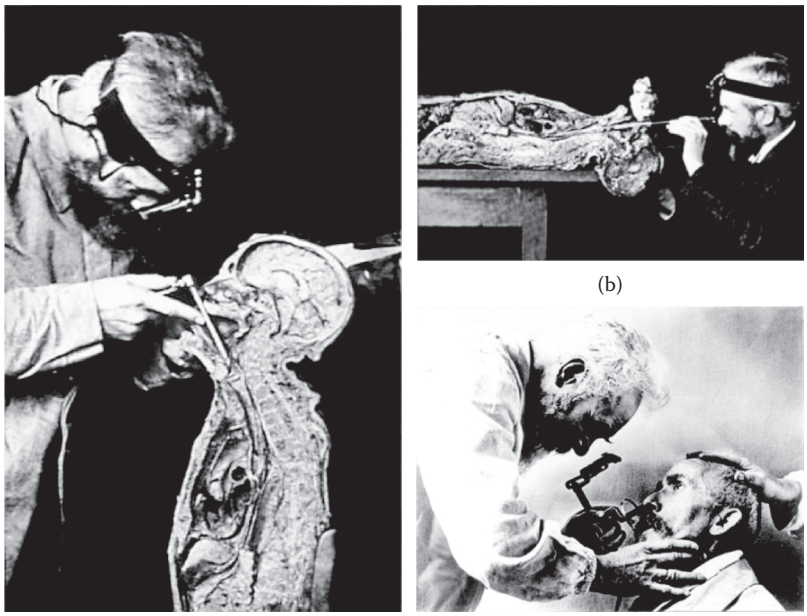

(a) (b) (c)

FIGURE 16.4
Dr. Gustav Killian and the first rigid bronchoscope. ((a and b) From Becker and Marsh, copyright Karger, Basel, 2000. With permission. (c) From public domain: http://en.wikipedia.org/wiki/File:Killian.jpg.)

stuck in the right main bronchus of a 63-year-old man (Becker and Marsh, 2000). Figure 16.4 shows pictures of Dr. Killian and his pioneering technique.

A rigid bronchoscope is thus a straight, hollow, metal tube through which a rigid fiber-optic device is placed, providing access to the central airways. The tube can only be inserted through the mouth and requires general anesthesia. It was the standard procedure for airway assessment until the 1970s, when the flexible bronchoscope was introduced. Today, it remains the procedure of choice for the removal of foreign objects from the airways or when a larger biopsy is needed. The rigid bronchoscope is also essential for the insertion of silicone or other stents, since it provides the necessary working channel for the insertion and removal of the tubes (Prakash, 1999).

16.3.2 Flexible Bronchoscopy

In the late 1960s, Dr. Shigeto Ikeda introduced the flexible bronchoscope, which aimed to reach further segments of the airway and to have a constant light source at the distal tip of the tube to enhance illumination of the visited areas. Later, in the late 1980s, Dr. Ikeda was also the one to introduce the videobronchoscope, which projected magnified images of the airways on a display (Miyazawa, 2000). The flexible bronchoscope became common since its introduction, and today, it is the most used invasive technique in the study of the airways (Prakash, 1999). Figure 16.5 shows Dr. Ikeda using the flexible bronchoscope.

The flexible bronchoscope is a thin flexible device that carries an optic fiber to conduct light from an external light source. It also contains an optical system to enable the visualization of the airway structures through an eyepiece or an image display. Auxiliary tools can also be inserted through the tube, commonly used for the collection of samples and

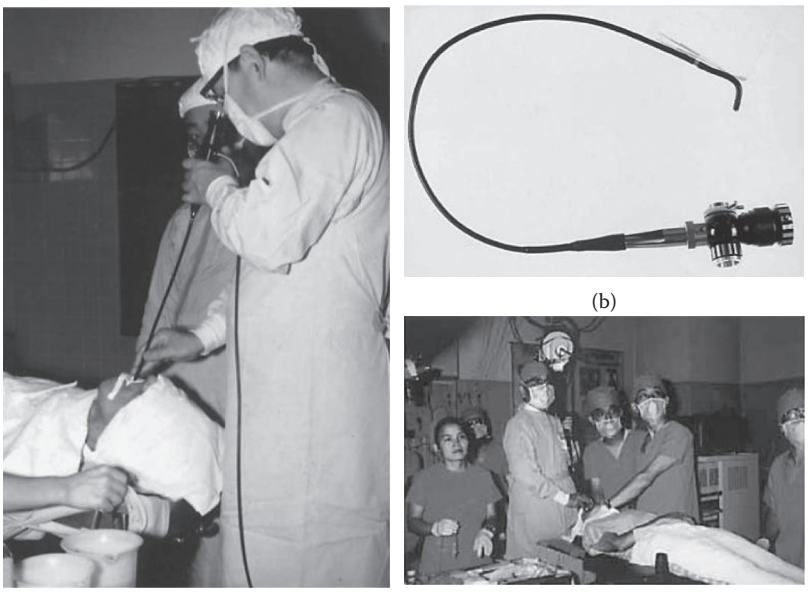

(a) (b) (c)

FIGURE 16.5
(a) Dr. Shigeto Ikeda, (b) the flexible bronchoscope, and (c) the video bronchoscope in the operating theater. (From Miyazawa, copyright Karger, Basel, 2000. With permission.)

therapy. Besides the ability of reaching further areas of the airways, one advantage of the flexible bronchoscope over the rigid bronchoscope is that it generally requires only local anesthesia and mild patient sedation if necessary (Prakash, 1999; Miyazawa, 2000).

As an example of the employment of flexible videobronchoscopy in the assessment of the airways, Czaja et al. (2007) used a computer program through which the recorded images could be measured. Figure 16.6 shows the application in use. A probe with known dimensions was used in the calibration of the program, and the areas of interest could then be measured by manual delineation.

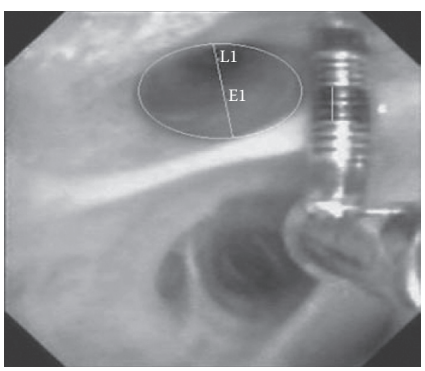

FIGURE 16.6
Airway measurement using the flexible bronchoscope. (From Czaja et al. copyright Karger, Basel, 2007. With permission.)

16.4 Computer-Aided Methods

Despite the fact that the traditional methods above are still the gold standard in the management of tracheal stenosis, they do have limitations. Stephens and Wood (2000), for instance, reported cases in which flexible bronchoscopes were avoided in the evaluation of critically narrowed airways because of the potential for occlusion of the narrowed tracheal lumen. Furthermore, as mentioned in the previous section, both flexible and rigid bronchoscopy often require patient sedation and are invasive procedures by nature.

For these reasons, and followed by advances in imaging technology, noninvasive computer-aided methods for assessment of stenosis have been developed to substitute or complement the traditional techniques. Next, a number of different computer-aided methods are described and discussed.

16.4.1 Manual Methods

In the category of manual methods, the physician directly interacts with the images acquired for the patient evaluation. No computer methods are employed to aid the physician in assessing the stenosis or choosing a stent if one is to be used. Although radiography can still be used as an imaging modality, volume imaging is the preferred choice, with CT being the most often modality.

Williamson et al. (2010) and McLaughlin et al. (2008) employed a novel imaging technique called anatomical optical coherence tomography (aOCT) in the measurement of the tracheal caliber. Optical coherence tomography (OCT) is a light-based imaging technique in which receptors capture how much the light emitted from a source has been absorbed or scattered inside the analyzed tissue. aOCT is a modification of conventional OCT designed to allow macroscopic imaging of hollow organs. Light is emitted from a very thin probe (approximately 2 mm) passing through a flexible bronchoscope inside the trachea. The probe rotates at around 2.5 Hz, tracing an axial image of the airway. Longitudinal displacement of the probe inside the trachea eventually yields 3D reconstructions. Figure 16.7 shows examples of the acquired images. An advantage of aOCT over other imaging techniques is that it can be used for long periods, enabling physiological as well as anatomical analyses.

Callanan et al. (1997) were the first to use magnetic resonance imaging (MRI) to assess tracheal stenosis following tracheotomy in a study with 18 patients. The diameter of the trachea was measured in sagittal images at five separate intervals from the cricoid. If stenosis was noted, the narrowing was quantified as the percentage of reduction in the diameter relative to the regions immediately above and below the stenotic segment. The authors claimed that MRI was indeed an interesting imaging modality for the assessment of stenosis, providing good image quality and, compared with CT, it has the advantage of not subjecting the patient to ionizing radiation.

Despite the apparent advantages of MRI, the superior resolution and contrast of CT images and the much faster scanning times make CT the preferred imaging modality for tracheal and airway analysis. Lee et al. (2005), for example, used CT image analysis in the prestent and poststent placement settings. They emphasized how multislice CT provides invaluable information in the initial evaluation of patients presenting airway obstruction, being an important complementary tool to bronchoscopy. They further showed that CT aids planning of stent implants by clearly delineating the anatomy, pathology, and severity of the airway obstructions. As an added benefit, CT images show the relationship between

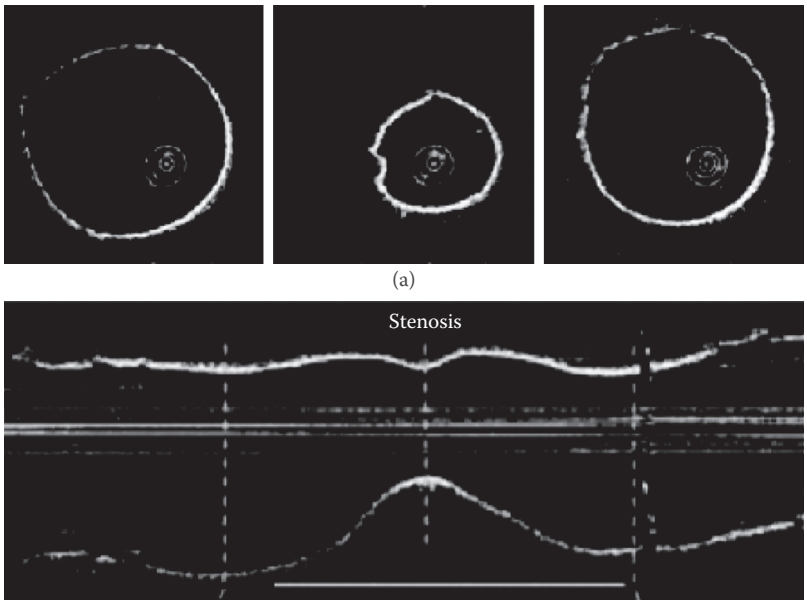

(a)

(b)

FIGURE 16.7
aOCT images of the trachea. (a) Cross sections obtained at different locations of the trachea. (b) Longitudinal displacement of the light probe along the trachea shows stenosis (the dashed lines correspond to the cross sections in (a)). (From Williamson et al. copyright *ERS Journals*, 2010. With permission.)

the central airways and the adjacent structures, which are not visible with the bronchoscope. In the poststent placement procedures, multislice CT proved to enable accurate detection of stent complications, including migration, size discrepancies, and fracture. The authors also referred to other successful cases reported in the literature.

More recently, Parida and Gupta (2008) demonstrated good correlation in assessment of stenosis between spiral CT with 3D reconstructions (SCT-3DI) and bronchoscopy. In this imaging modality, a 3D model of the trachea is generated from the CT data (see Figure 16.8). This improves over traditional multislice CT analysis, providing the physician with

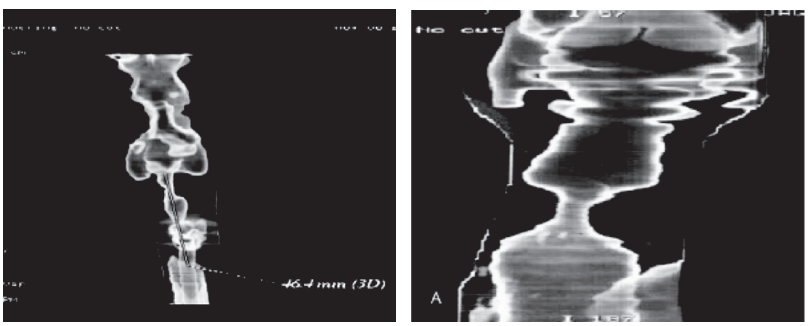

(a) (b)

FIGURE 16.8
3D models of the trachea obtained with SCT-3DI. (From Parida and Gupta, copyright Elsevier, 2008. With permission.)

volumetric information. The authors also reported that in 16 out of 30 cases, bronchoscopy could not measure the length of the stenosis due to severe narrowing. With SCT-3DI, all cases could be measured.

Another improvement obtained with image analysis is the use of virtual bronchoscopy, in which a virtual camera is controlled by the physician through a 3D reconstruction of the airways obtained from CT. In this way, bronchoscopy is simulated in a completely virtual environment. Such a technique has the advantage of being similar in procedure to rigid or flexible bronchoscopy, with which the physician tends to be familiar, but without being invasive.

For this reason, virtual bronchoscopy is often used in training. Ferguson and McLennan (2005) reviewed several application scenarios of virtual bronchoscopy, demonstrating current and future trends for the procedure. They described, for instance, how images captured with the bronchoscope can be correlated with those of virtual bronchoscopy. This augments the physician's view and enables the visualization of structures that would otherwise be hidden when using only bronchoscopy. In airway analysis, Shitrit et al. (2005) and Triglia et al. (2002) showed significant correlation between results obtained with virtual bronchoscopy and flexible bronchoscopy in the assessment of tracheal stenosis. Hoppe et al. (2004) also demonstrated that virtual bronchoscopy can even be used to grade stenosis of the airways down to the segmental levels. Figure 16.9 gives examples of the use of virtual bronchoscopy.

Finally, Ballester et al. (2009) recently proposed an interesting system for tracheal surgery planning and choice of stents. A graphical user interface (see Figure 16.10) enables the user to visualize the CT data, 3D reconstructions of the trachea, and volume-rendered images altogether. The stents are then chosen from a prebuilt database containing computer-aided detection models of commercially available tubes. These are manually overlaid on the images so that the physicians can have a better idea of how the stent will interact with the tracheal wall and neighbouring regions. The 3D reconstructions of trachea were also used for biomechanical airflow simulation studies before and after stent insertion.

All these methods have certainly proved the benefits of image analysis in the assessment of the airways and especially of tracheal stenosis. Yet, they are all still very reliant on the expertise of the operator in charge. The next section reviews methods that incorporate sophisticated algorithms aiming to reduce this operator dependency.

(a) (b)

FIGURE 16.9
Virtual bronchoscopy. (a) Normal (left) and narrowed (right) tracheas as seen with the virtual camera. (From Shitrit et al. copyright American College of Chest Physicians, 2005. With permission.) (b) Stenosis caused by tumour seen at the main bronchus. (From Hoppe et al. copyright American College of Chest Physicians, 2004. With permission.)

FIGURE 16.10
Graphical user interface for the planning of stent insertions. The stents are taken from a database and manually placed in the image. (From Ballester et al. copyright Springer Berlin, 2009. With permission.)

16.4.2 Semiautomatic Methods

To the best of our knowledge, all semiautomatic algorithms devoted to the assessment of tracheal stenosis share the same characteristic. Namely, their output is a graph or some other interface to convey to the clinician the variation in the cross-sectional diameter or area of the trachea. What is different between these algorithms is how they achieve such results, which may involve more or less user intervention.

The first step in this process is the segmentation of the trachea from the CT image data and, possibly, its conversion to a 3D surface. Graham et al. (2000) presented a study with eight patients in which several image-based techniques employed to assess and measure the airways. They employed the software presented by D'Souza et al. (1996) and Hoffman et al. (1992) to segment the airways and extract their center lines. In the software, segmentation is semiautomatically performed on a slice-by-slice basis: rays cast from a user-defined point near the barycenter of the airway lumen determine the location of inner and outer airway walls. This information is also used to segment the lumen with region growing. Figure 16.11 illustrates some results obtained with these methods.

Triglia et al. (2002) also segmented the trachea on a slice-by-slice basis but used two-dimensional (2D) active contours (Kass et al. 1988) to delineate the axial boundary between the tracheal wall and the lumen. In their approach, user intervention is potentially reduced by selecting only the first and last slices of the trachea, segmenting the first slice, and letting the algorithm use the result of each slice as the starting point for the next. After the segmentation, new contours perpendicular to the surface's center line are computed and used in the definition of a smooth B-spline surface. The operator then marks on the center line the start and end of the stenosis, which are used to compute the length of the narrowing. The degree of narrowing is finally computed as the ratio of the cross-sectional area of the selected tracheal segment to the area of a reference healthy section also selected by

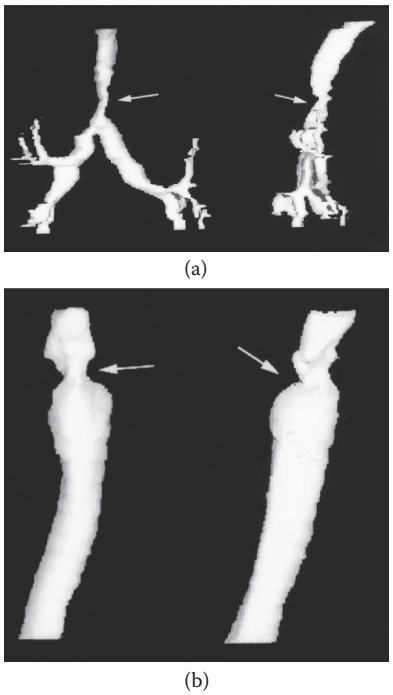

FIGURE 16.11
Examples of 3D reconstructions of the trachea and airways showing stenosis. (From Graham et al. copyright W.B. Saunders, 2000. With permission.)

the operator. The area or diameter profile of the entire trachea can further be displayed on a graph, accompanied by a visualization of the 3D surface. Figure 16.12 shows a couple of steps of this algorithm.

I actively referred to Triglia's procedure correct?

In the studies of Valdés-Cristerna et al. (2000) and Valdés-Cristerna and Yáñez-Suárez (2003), a 3D contour model was employed in the segmentation of the trachea. This improves Triglia et al.'s (2002) procedure by eliminating the surface generation step, since the 3D model already tends to yield a smooth 3D surface by definition. Triglia et al. (2002) also reported difficulties in the slice-by-slice segmentation whenever the narrowing was too severe and the tracheal lumen was barely visible in the image. In these cases, the missing tracheal section had to be reconstructed manually, which can obviously introduce errors. Although the 3D contour model can potentially overcome this problem, Valdés-Cristerna et al. (2000) and Valdés-Cristerna and Yáñez-Suárez (2003) did not report any result related to such situation. The tracheal area profile was once again plotted on a graph, but details on this process were not given either.

In the method presented by Sorantin et al. (2002, 2006), the cross-sectional area profile of the trachea is obtained by first segmenting the trachea with a region growing method using fuzzy connectedness (Udupa and Samarasekera, 1996). Next, a thinning algorithm (Palágyi and Kuba, 1998) is applied to the segmentation result to extract the trachea's center line. Both steps may require postprocessing by user intervention. As in the other discussed approaches, the tracheal area profile is plotted on a graph, and the start and end of

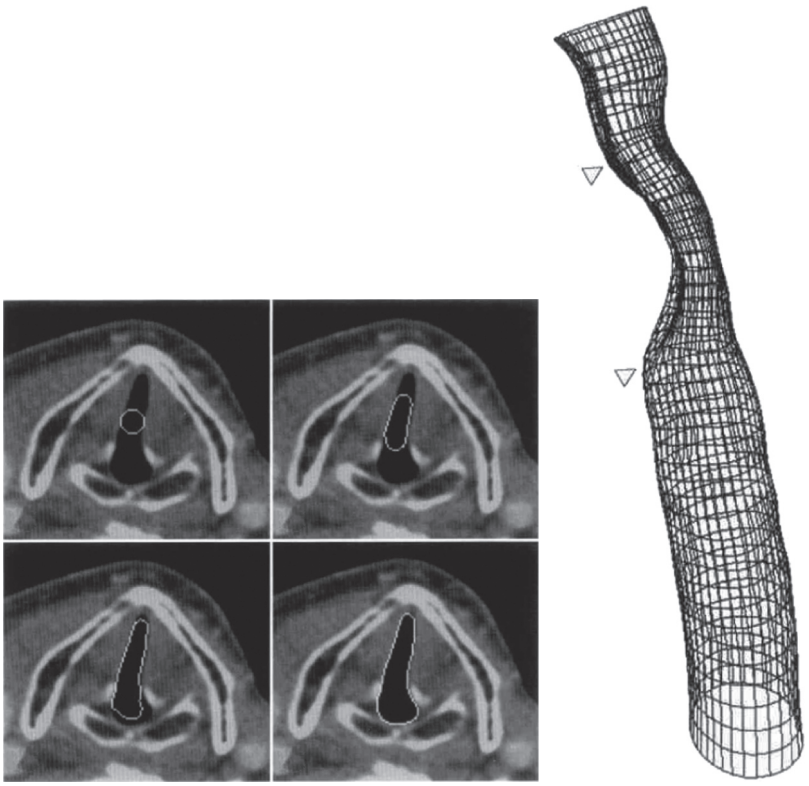

(a) (b)

FIGURE 16.12
(a) Segmentation of an axial CT slice using active contours. (b) 3D surface obtained from the segmentation with user markers indicating the start and end of the stenosis. (From Triglia et al. copyright Annals Publishing Company, 2002. With permission.)

the stenosis are determined by the operator based on this graph and its relationship with the 3D reconstruction of the trachea. The degree of narrowing is chosen as a percentage of the minimum cross-sectional area relative to the area of the trachea at the start and end points of the stenosis. Kiesler et al. (2007) later used this method for the assessment of three patients. Figure 16.13 illustrates the method and its results.

The improvements brought about by all these techniques over the manual methods are undeniable. Nonetheless, the methods above share another common characteristic: the analysis of the result graph and the determination of the parameters of the stenosis are still, to a large extent, operator-dependent. Although the visualization of the tracheal area profile on a graph does ease the assessment, it is the operator that decides where the stricture starts and ends, and the degree of narrowing is eventually computed from these parameters. In addition, in the case of stent choice, it is not completely clear from the graphs how much the stent should push the tracheal wall, that is, how to decide the appropriate stent diameter to be employed. In the end, it is the physician that still needs to guess the healthy tracheal shape from the available results in order to choose the correct stent.

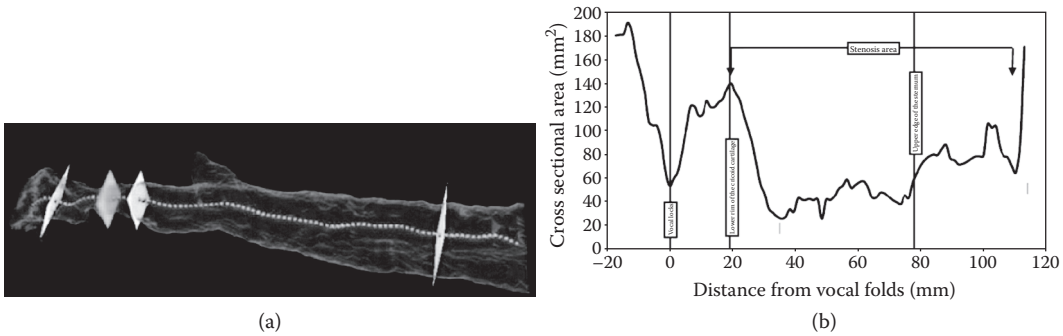

FIGURE 16.13
(a) The trachea with the center line and cross sections whose areas are computed. (b) The area profile along the trachea. (From Kiesler et al. copyright Springer, New York, 2007. With permission.)

16.4.3 Deformable Models

This section describes a new method to further improve the assessment and stenting of tracheal stenosis based on deformable models of shape. In this method, a statistical shape model (Cootes et al. 1995) of healthy tracheas is used to estimate the shape of a patient's trachea in case stenosis was not present. From there, an adapted active contour model (Kass et al. 1988) is used to segment the narrowed trachea from the patient's CT scan. Both healthy and narrowed versions of the trachea are then used in the automatic detection of the stenosis and its parameters (start, end, degree of narrowing). These parameters are finally used for an automatic suggestion of the appropriate outer diameter and length of the stent. The details of this approach are given in the following.

16.4.3.1 Estimation of Healthy Tracheas

An active shape model (ASM), as defined by Cootes et al. (1995), is a statistical model of shapes whose objective is to capture the geometric variation present in a set of training shapes. This model is then capable of generating new shape instances that are constrained by the statistical variation of the training set, referred to as the allowable shape domain. As a result, a defining characteristic of ASMs, an advantage with respect to other deformable models, is that they can only generate shapes that resemble those in the training set.

This characteristic is the motivation to use an ASM of healthy tracheas to estimate the shape of a patient's trachea if stenosis was not present. Since the model contains only instances of healthy tracheas, local geometric variations typical of stenosis cannot be generated. In this way, the physician can have visual and mathematical guidance of what shape the trachea should have after treatment, with either surgery or stent implants.

The steps involved in the construction of the ASM and its registration to a patient's CT scan are described in the following.

> **Training set.** An ASM is built from a set of training shapes. In medical imaging, these are usually obtained through segmentation. In the case of the trachea, any algorithm that can segment the tube from beginning (region right below the cricoid) to end (region of the carina) will do. In particular, Pinho et al. (2009) proposed an adaptive airway segmentation algorithm capable of yielding such results.

Furthermore, this algorithm also obtains an approximation of the trachea's center line.

The points (or landmarks) defining the boundary of the shapes of the training set must have a one-to-one correspondence so that the ASM captures correct shape variations. The correspondences along the center lines obtained with the segmentation algorithm above are achieved with arc-length parametrization. From the center lines, smooth 3D representations of the boundaries of the tracheas can be obtained by regularly sampling the segmentations around the center line points. This procedure eventually yields the required point correspondence.

Active shape model. After establishing the correspondences between the N shapes of training set, each shape $\mathcal{S}_i$ has its set of landmarks $\mathcal{X}_i$ converted into a $3n$-dimensional vector $\mathbf{x}_i = (x_{i11},x_{i12},x_{i13},\ldots,x_{in1},x_{in2},x_{in3})^{\mathrm{T}}$. The tracheas are then aligned with respect to location and pose and normalized with respect to scale, such that $|\mathbf{x}_i| = 1$. Principal component analysis extracts the eigenvectors, $\mathbf{p}_i$, and eigenvalues, λ_i, of the covariance matrix of all $\mathbf{x}_i$'s. The eigenvectors, also referred to as the main modes of variation of the training set, are grouped in an orthonormal matrix $\mathbf{P}_{3n\times N}$. New healthy tracheas can be generated with this model, called a *point distribution model*, by linearly combining the mean shape with a weighted version of the eigenvector matrix **P**, that is,

$$\mathbf{x} = \bar{\mathbf{x}} + \mathbf{Pb}. \tag{16.1}$$

Vector $\mathbf{b} = (b_1,b_2,\ldots,b_N)^{\mathrm{T}}$ is the set of parameters of the model and represents the contribution of each eigenvector. Since λ_i represents the variance of the training set along the eigenvector $\mathbf{p}_i$, the range $[-3\sqrt{\lambda_i}, +3\sqrt{\lambda_i}]$ is a suitable limit for b_i (Cootes et al. 1995).

In general, only the first t modes corresponding to a certain percentage of the total variance present in the point distribution model are used. The rest of the modes are considered as noise (Cootes et al. 1995). As an example, Figure 16.14

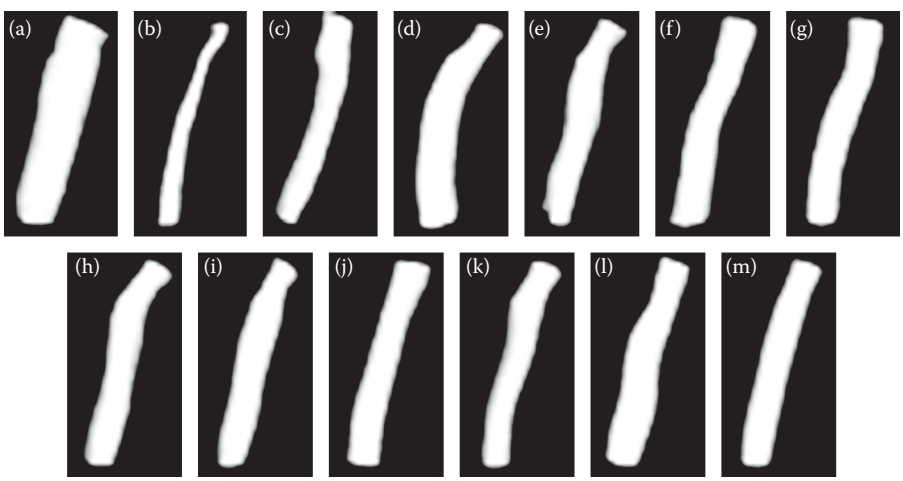

FIGURE 16.14
(a–f), The first six modes of variation of an example ASM built with 38 healthy tracheas. Each figure shows the (middle) average shape, (left) $-3\sqrt{\lambda_i}$, and (right) $+3\sqrt{\lambda_i}$ along the mode.

shows the first six modes of variation computed for a training set of 38 healthy tracheas. The average shape is shown in the middle, and the shapes corresponding to $\pm 3\sqrt{\lambda_i}$ appear next to it. The mode with largest variation indicates changes in the caliber. The second mode represents global bending, and from then onward, different levels of local bending or twisting.

ASM registration. ASMs can be registered to an object of the class they represent by adjusting the parameter vector **b**. When the ASM is registered to an image, the registration is usually implemented as an iterative edge based search. Fitting an ASM of healthy tracheas to a stenotic trachea is a challenge in itself. The difficulty lies in the fact that the narrowed regions of the trachea may have a strong influence on the fitting process. To avoid such an influence, the registration of the ASM of healthy tracheas is subdivided in steps. It consists of an initialization step (whose aim is to scale, orient, and place the mean shape so that it is near the target in the image), followed by rigid and nonrigid registration stages. In the latter two, the landmarks of the shape generated by the model, **x**, are moved along their normals toward high gradients corresponding to edges of the target, generating a candidate shape **y**. In the rigid registration, the average shape of the model is rigidly aligned with the target trachea in the image. The nonrigid registration is described next.

Pose and shape registration. In the second stage of the ASM registration, a nonrigid registration, which optimizes pose and shape, is started, and the landmarks of the shape generated by the model at the current iteration are displaced along their normals. Once the candidate shape **y** is projected into model space, which aligns **y** with the average shape, a new set $\hat{\mathbf{b}}$ that defines the best fit of the model to **y** is obtained by minimization of the squared error between **y** and **x**, represented by the following error function:

$$\xi(\mathbf{b}) = (\mathbf{y} - \mathbf{x})^{\mathrm{T}}(\mathbf{y} - \mathbf{x}). \tag{16.2}$$

Expanding Equation 16.2 with Equation 16.1 and minimizing ξ with respect to **b** results in:

$$\hat{\mathbf{b}} = \mathbf{P}^{\mathrm{T}}(\mathbf{y} - \bar{\mathbf{x}}). \tag{16.3}$$

This minimization is herein referred to as StandardLS. A new shape $\hat{\mathbf{x}}$ is generated from $\hat{\mathbf{b}}$, using Equation 16.1 and is transformed back into the image space. The displacement of landmarks and the update of **b** and $\hat{\mathbf{x}}$ are repeated until no significant changes are made to $\hat{\mathbf{x}}$ (Cootes et al. 1995).

Fixed landmarks. Although the registration of the model of healthy tracheas to a trachea with stenosis tends not to be affected by the local geometric variations of the stricture, the registration may still produce globally narrowed tracheas. This result is possible because, as shown in Figure 16.14, global narrowing may be an integral part of the geometric variations present in the model. The fixed landmarks registration method overcomes this problem by setting a restriction on the displacement of landmarks during the search for high gradients, which defines the candidate shape **y**. Namely, if the candidate locations are not within a short

threshold distance $d > 0$ from $\mathbf{x}$, the corresponding landmarks of $\mathbf{y}$ remain fixed, while the other landmarks are allowed to move as usual.

Let $\hat{\mathbf{x}}^{(k)} = \bar{\mathbf{x}} + \mathbf{P}\hat{\mathbf{b}}^{(k)}$ be the shape generated by the model at iteration k of the non-rigid registration. Let $\mathbf{y}^{(k+1)}$ be the candidate shape generated by displacing the landmarks of $\hat{\mathbf{x}}^{(k)}$, assuming that $\mathbf{y}^{(k+1)}$ has already been projected into model space and aligned with $\bar{\mathbf{x}}$. Using the fixed landmarks principle, the parameters $\hat{\mathbf{b}}^{(k+1)}$ are given by

$$\hat{\mathbf{b}}^{(k+1)} = \left[\mathbf{P}^T(\mathbf{y}^{(k+1)} - \bar{\mathbf{x}})\right]\Big|_{\mathcal{L}'} + \left[\mathbf{P}^T(\hat{\mathbf{x}}^{(k)} - \bar{\mathbf{x}})\right]\Big|_{\mathcal{L}''}, \tag{16.4}$$

in which $\mathcal{L}'$ is the set of landmarks for which the displacement with respect to $\hat{\mathbf{x}}^{(k)}$ was longer than d, whereas $\mathcal{L}''$ are the landmarks that remained fixed because the displacement was shorter than or equal to d.

Equation 16.4 therefore shows that $\hat{\mathbf{b}}^{(k+1)}$ is determined by both the displaced landmarks $\mathbf{y}^{(k+1)}|_{\mathcal{L}'}$ and the landmarks $\hat{\mathbf{x}}^{(k)}|_{\mathcal{L}''}$, which remained fixed. Consequently, when computing

$$\hat{\mathbf{x}}^{(k+1)} = \bar{\mathbf{x}} + \mathbf{P}\hat{\mathbf{b}}^{(k+1)}, \tag{16.5}$$

$\hat{\mathbf{x}}^{(k+1)}$ will be the best fit, in a least squares minimization sense, to $\mathbf{y}^{(k+1)}|_{\mathcal{L}'}$ and $\hat{\mathbf{x}}^{(k)}|_{\mathcal{L}''}$. Figure 16.15 illustrates the whole concept. Provided that there are enough healthy areas around regions with stenosis, the fixed landmarks force the shape generated by the model to remain far from those regions, while enabling correct

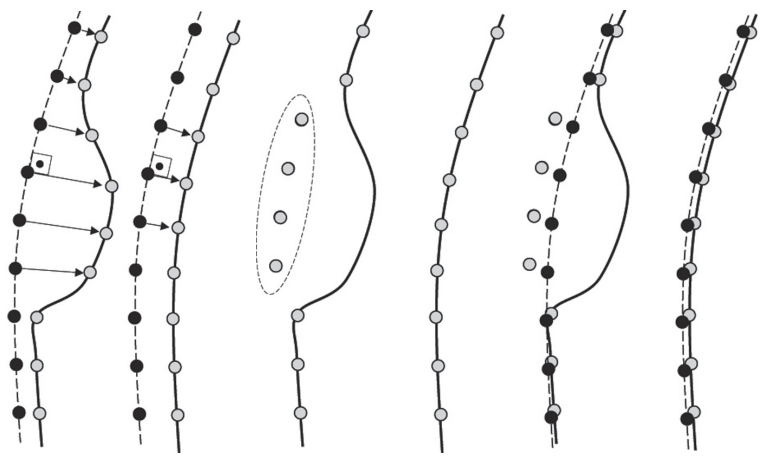

FIGURE 16.15
The fixed landmarks concept: (a) $\hat{\mathbf{x}}^{(k)}$ (dashed) is attracted by high gradients of the stenotic trachea in the image (thick lines)—the arrows indicate the landmark displacements $d\mathbf{y}^{(k+1)}$; (b) the set of landmarks that remain fixed, $\hat{\mathbf{x}}^{(k)}|_{\mathcal{L}''}$, because the displacement was longer than d. (c) $\hat{\mathbf{x}}^{(k+1)}$—the fixed landmarks keep the shape far from the stenotic area.

matches at the healthy areas. As the shape deforms iteratively, it progressively assumes the form of the desired healthy trachea, guided by the regions where correct matches occur.

16.4.3.2 Segmentation of Narrowed Tracheas

ACMs, commonly known as snakes, are curves defined within an image domain that are able to move under the influence of internal forces derived from the curve itself and of external forces derived from the image data. The internal and external forces are defined in such a way that the curve will register to an object boundary or other desired features within an image. As defined by Kass et al. (1988), a snake can be represented in 2D by a curve $\mathbf{v}(s) = (x(s),y(s))$, $s \in [0,1]$, responding to an energy functional of the form:

$$E = \int_0^1 [\kappa E_{int}(\mathbf{v}(s)) + (1-\kappa)E_{ext}(\mathbf{v}(s))]\,\mathrm{d}s, \tag{16.6}$$

where $\kappa \in [0,1]$ is a weighting factor.

The internal energy E_{int} commonly restricts the deformations taking into account curvature and elasticity. Considering elasticity, the functional prevents the curve from breaking apart, maintaining its continuity. As for elasticity, the internal energy avoids the appearance of sharp corners. The external energy represents the gradient of an image I convolved with a Gaussian function G at scale σ, which causes the curve to be attracted by contours with high image gradients.

The objective is then to minimize Equation 16.6, making the system a force balance equation of the form:

$$\mathbf{F}_{\text{int}} + \mathbf{F}_{\text{ext}} = 0, \tag{16.7}$$

where

$$\mathbf{F}_{\text{int}} = -\nabla E_{\text{int}} \tag{16.8}$$

and

$$\mathbf{F}_{\text{ext}} = -\nabla E_{\text{ext}}. \tag{16.9}$$

The minimization is solved iteratively, often in the discrete domain after discretization of $\mathbf{v}(s)$. The expected result is a curve that matches the high gradients of the image while being restricted by the internal constraints, according to the assigned weighting factors.

A classical problem with ACMs, however, is initialization. The starting curve should be placed near the features to be detected in the image; otherwise, the capture range of the external energy may not extend enough to attract the curve. In addition, in the absence of external energies, the internal energies cause the curve to shrink into itself.

Several methods have been proposed to overcome the limitations of the original ACM formulation. Cohen (1991), for instance, added a balloon force to the energy formulation that pushes the curve outwards in the direction of its normals, avoiding it to shrink. Later,

Cohen and Cohen (1993) proposed to increase the capture range of the external energy by using a force based on a map of distances from any point in the image to the nearest edge. The gradient vector flow of Xu and Prince (1998) and the recent magnetostatic active contour model of Xie and Mirmehdi (2008) are other good examples of methods that affect the external force.

The concepts above naturally extrapolate to 3D and can easily be adapted to a discrete domain. Within the context of the proposed application, a discrete surface is defined as $\mathcal{S} = (\mathcal{X},\mathcal{T})$, where $\mathcal{X}$ is the set of points or landmarks, with $\mathbf{x}_{v_j}$, $j = 1,\ldots,n$, a point in this set, and $\mathcal{T}$ is the set of triangles connecting the points of $\mathcal{X}$.

The ACM is initialized with the estimation of the healthy shape of the trachea obtained with the ASM above. In this way, the initial shape tends to be near enough to the boundary of the narrowed trachea in the image. The deformation algorithm then iteratively loops through all the points in $\mathcal{X}$, applying the ACM forces locally, until no significant deformation has been made to the surface. Below, the internal and external forces are briefly presented.

External force. The ideas first presented by Cohen and Cohen (1993) are adapted to create an external force to guide the deformation of the surface. At first, the original image, I, is thresholded to segment air (at −200 Hounsfield units), after which the result is inverted. This will generate two binary images, I_{B1} and I_{B2}. Next, a 3–4–5 chamfer distance transform is applied to each binary image, yielding two distance maps, I_{D1} and I_{D2}, respectively. Both distance transforms are combined into a new distance map $I_D = I_{D1} + I_{D2}$.

Eventually, the external force term of Equation 16.7 applied to the landmark $\mathbf{x}_{v_j}$ of $\mathcal{X}$ is defined as

$$\mathbf{F}_{\text{ext}_j} = -\frac{|\nabla I_D(\mathbf{x}_{v_j})|}{M}\nabla I_D(\mathbf{x}_{v_j}), \tag{16.10}$$

where M is the maximum gradient magnitude in I_D.

Internal forces. The internal force $\mathbf{F}_{\text{int}}$ controls stretching and bending, in such a way that the surface is continuous (does not break apart) and remains smooth (has no sharp corners). The force tries to keep the landmarks equally spaced and tries to minimize the local Gaussian curvature of the surface. It is given by

$$\mathbf{F}_{\text{int}_j} = \gamma\, \mathrm{F}_{\text{elast}_j} + (1-\gamma)\mathbf{F}_{\text{be}}$$ (16.11)

where γ is a weighting factor.

$\mathbf{F}_{\text{elast}}$ is the elastic force applied to $\mathbf{x}_{v_j}$ of $\mathcal{X}$, defined as:

$$\mathbf{F}_{\text{elast}_j} = D_j \frac{\mathbf{d}_{\text{elast}_j}}{|\mathbf{d}_{\text{elast}_j}|}, \tag{16.12}$$

where the directional component $\mathbf{d}_{\text{elast}}$ moves the landmark toward a central point relative to its neighbours. The scalar component D_i, in turn, is a normalized measure of how much $\mathbf{x}_{v_j}$ deviates from this central point.

The bending force $\mathbf{F}_{\text{bend}_j}$ is given by

$$\mathbf{F}_{\text{bend}_j} = K_{G_j} \frac{\mathbf{d}_{\text{bend}_j}}{|\mathbf{d}_{\text{bend}_j}|}, \tag{16.13}$$

where $\mathbf{d}_{\text{bend}_j}$ is either equal to $\mathbf{d}_{\text{bend}_j}$ or it moves $\mathbf{x}_{\text{v}_j}$ along its normal if the landmark is not located at the open ends of the surface. In either case, the directional component moves $\mathbf{x}_{\text{v}_j}$ in such a way that the discrete Gaussian curvature computed at the landmark is minimized. The scalar component K_{G_j} is a normalized measure of how much the curvature at $\mathbf{x}_{\text{v}_j}$ deviates from zero.

Finally, for each iteration k of the deformation algorithm of the ACM, the landmarks of the surface are updated as follows:

$$\mathbf{x}_{\text{v}_j}^{(k)} = \mathbf{x}_{\text{v}_j}^{(k-1)} + \kappa \mathbf{F}_{\text{int}_j} + (1-\kappa)\mathbf{F}_{\text{ext}_j}. \tag{16.14}$$

16.4.3.3 Quantification of Stenosis

Once healthy and narrowed versions of the trachea are obtained, the assessment of the stenosis is straightforward. This is achieved by comparing the cross-sectional area profile of the two surfaces along their center lines. The narrowed surface is first intersected with the planes corresponding to the boundary contours of the healthy surface. The area of the generated set of contours is then compared with the area of the set of contours of the healthy surface. If a decrease in the area ratio between healthy and narrowed tracheas is detected, there is an indication that stenosis is present. Two thresholds must be set in this process: L_0 determines the minimum length of the detected stenosis and avoids very short segments to be considered; $R_0 \in [0,1]$ determines the maximum area ratio to be considered, balancing false-positive and detection rates of stenosis. Thus, the path that is longer than L_0 along which the area ratio is smaller than R_0 is recorded, which determines the start and end of the stenosis. The point with the lowest ratio is finally chosen as the one that determines the degree of narrowing of the stricture.

Examples of the stenosis assessment for six patients obtained with the method above are shown in Figure 16.16. Note that the detected parameters of the stenosis conform to the diagnostic details shown in the figure.

16.4.3.4 Choice of Stents

The stent parameters are directly obtained from the algorithm above. The caliber of the stent is the average diameter of all contours of the estimated healthy surface along the extent of the stenosis. The deployment location is equal to the start point. Finally, the length of the stent is the path length between the start and end points. Figure 16.17 shows examples of predicted stents for the patients of Figure 16.16. The stents are directly derived from the computed parameters of the stenosis, as described above. They cover the stenosis according to the threshold ratio R_0 set for the detection of stenosis and provide a plausible healthy caliber for the narrowed trachea.

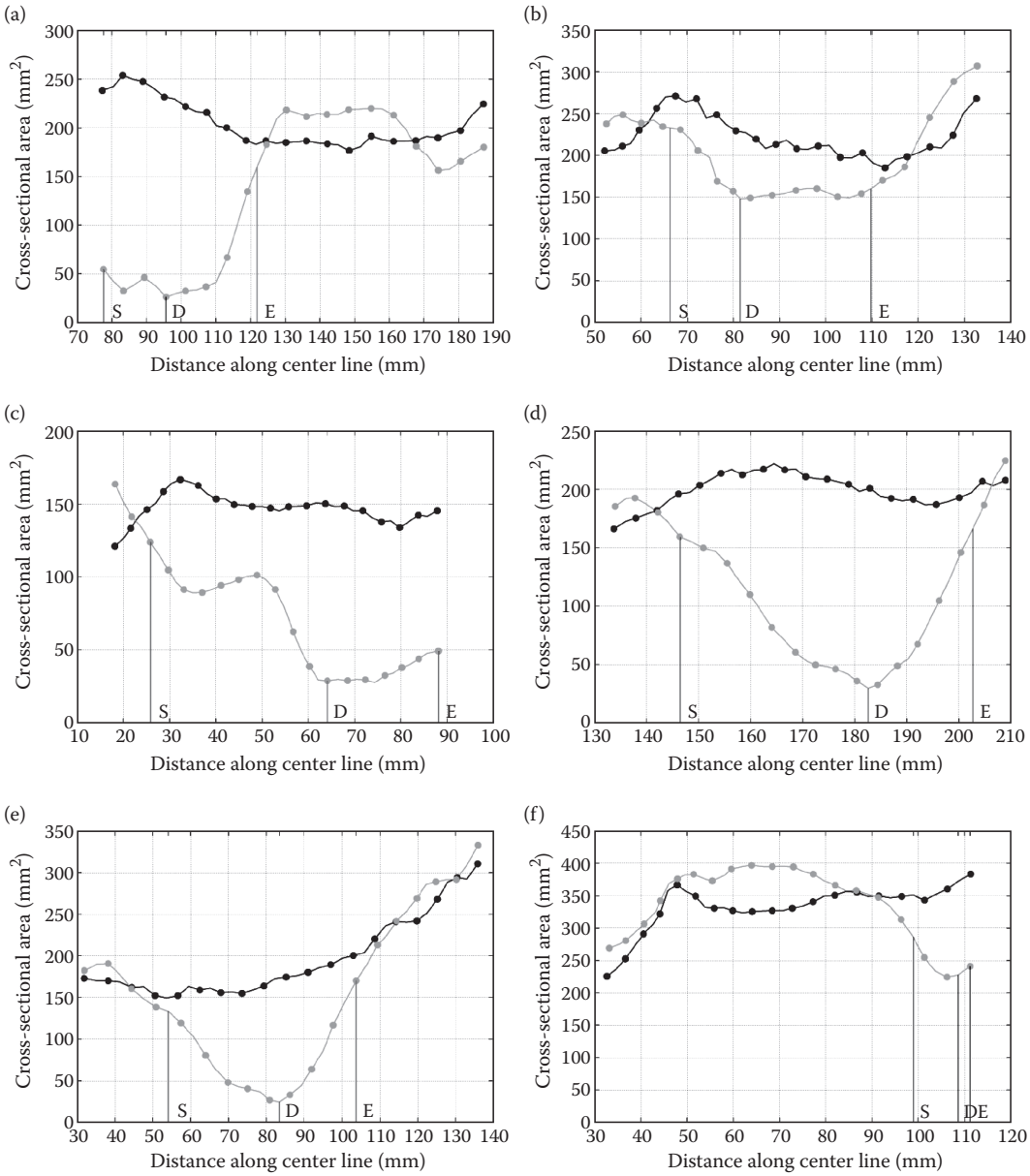

FIGURE 16.16
Examples of stenosis quantification for six patients. The vertical lines indicate the detected start, point of maximum degree, and end of the stenosis. The *x*-axis represents the distance along the center line of the trachea, where 0 marks the top (region around the cricoid).

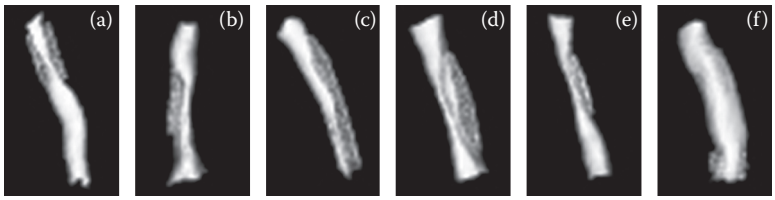

FIGURE 16.17
Visualization of the stents computed for the six patients in the examples.

16.5 Conclusions

Correct assessment of tracheal stenosis and subsequent choice of the length and diameter of stents are important preoperative steps in the management of the strictures. Assessment of tracheal stenosis and choice of tracheal stents, however, have long been very operator-dependent tasks. This chapter reviewed traditional and computer-aided methods for the assessment of tracheal stenosis and choice of stents. It has been shown that image analysis is a powerful noninvasive tool to complement the traditional bronchoscopic methods. In addition, computer-aided methods can greatly reduce the subjectivity and operator dependency usually observed in the assessment of tracheal stenosis. In particular, this chapter also described in detail a novel method to automatically assess stenoses and predict the diameter and length of stents using deformable models of shape.

References

M. A. G. Ballester, A. P. del Palomar, J. L. L. Villalobos, L. L. Rodríguez, O. Trabelsi, F. Pérez, Ángel Ginel Cañamaque, E. B. Cortés, F. R. Panadero, M. D. Castellano, and J. H. Jover. Surgical planning and patient-specific biomechanical simulation for tracheal endoprostheses interventions. *Medical Image Computing and Computer-Assisted Intervention—MICCAI 2009*, *Lecture Notes in Computer Science*, vol. 5762, pp. 275–282. Springer, New York, 2009.

H. D. Becker and B. R. Marsh. History of the rigid bronchoscope. In C. T. Bolliger and P. N. Mathur, editors, *Interventional Bronchoscopy*, vol. 30, pp. 2–15. Karger, Basel, 2000.

P. M. Boiselle, J. Catena, A. Ernst, and D. A. Lynch. Tracheobronchial stenoses. In P. M. Boiselle and D. Lynch, editors, *CT of the Airways*, pp. 121–149. Humana Press–Springer, New York, 2008.

V. Callanan, K. Gillmore, S. Field, and A. Beaumont. The use of magnetic resonance imaging to assess tracheal stenosis following percutaneous dilatational tracheostomy. *Journal of Laryngology and Otology*, 111(10):953–957, 1997.

A. Carretta, G. Melloni, P. Ciriaco, L. Libretti, M. Casiraghi, A. Bandiera, and P. Zannini. Preoperative assessment in patients with postintubation tracheal stenosis. *Surgical Endoscopy*, 20(6):905–908, 2006.

W. Ching-Yang, L. Yun-Hen, H. Ming-Ju, W. Yi-Chen, L. Ming-Shian, K. Po-Jen, and L. Hui-Ping. Airway stents in management of tracheal stenosis: Have we improved? *ANZ Journal of Surgery*, 77:27–32(6), 2007.

L. Cohen and I. Cohen. Finite-element methods for active contour models and balloons for 2-d and 3-d images. *IEEE Transactions on Pattern Analysis and Machine Intelligence*, 15(11):1131–1147, Nov. 1993.

L. D. Cohen. On active contour models and balloons. *Computer Vision, Graphics, and Image Processing: Image Understanding*, 53(2):211–218, 1991.

T. F. Cootes, C. J. Taylor, D. H. Cooper, and J. Graham. Active shape models: Their training and application. *Computer Vision and Image Understanding*, 61(1):38–59, 1995.

P. Czaja, J. Soja, P. Grzanka, A. Miel, A. Szczeklik, and S. K. Assessment of airway caliber in quantitative videobronchoscopy. *Respiration*, (74):432–438, 2007.

N. D. D'Souza, J. M. Reinhardt, and E. A. Hoffman. ASAP: Interactive quantification of 2d airway geometry. *Medical Imaging 1996: Physiology and Function from Multidimensional Images*, vol. 2709, pp. 180–196. SPIE, 1996.

M. Elliott, D. Roebuck, C. Noctor, C. McLaren, B. Hartley, Q. Mok, C. Dunne, N. Pigott, C. Patel, A. Patel, and C. Wallis. The management of congenital tracheal stenosis. *Advances in Pediatric ORL. Proceedings of the 8th International Congress of Pediatric Otorhinolaryngology. International Congress Series*, 1254:321–334, 2003.

J. S. Ferguson and G. McLennan. Virtual bronchoscopy. *Proceedings of the American Thoracic Society*, 2(6):488–491, 2005.

L. Freitag. Tracheobronchial stents. In C. T. Bolliger and P. N. Mathur, editors, *Interventional Bronchoscopy*, vol. 30, pp. 171–186. Karger, Basel, 2000.

L. Freitag. Airway stents. *Interventional Pulmonology*, vol. 48, pp. 190–217. ERS, 2010.

S. M. Graham, G. McLennan, G. F. Funk, H. T. Hoffman, T. M. McCulloch, J. Cook-Granroth, and E. A. Hoffman. Preoperative assessment of obstruction with computed tomography image analysis. *American Journal of Otolaryngology*, 21(4):263–270, 2000.

H. C. Grillo. *Surgery of the Trachea and Bronchi*. BC Decker, 2004.

H. C. Grillo, D. M. Donahue, D. J. Mathisen, J. C. Wain, and C. D. Wright. Postintubation tracheal stenosis: Treatment and results. *Journal of Thoracic and Cardiovascular Surgery*, 109(3):486–493, 1995.

E. A. Hoffman, D. Gnanaprakasam, K. B. Gupta, J. D. Hoford, S. D. Kugelmass, and R. S. Kulawiec. Vida: An environment for multidimensional image display and analysis. *Biomedical Image Processing and Three-Dimensional Microscopy*, vol. 1660, pp. 694–711. SPIE, 1992.

H. Hoppe, H.-P. Dinkel, B. Walder, G. von Allmen, M. Gugger, and P. Vock. Grading airway stenosis down to the segmental level using virtual bronchoscopy. *Chest*, 125 (2):704–711, 2004.

M. Kass, A. Witkin, and D. Terzopoulos. Snakes: Active contour models. *International Journal of Computer Vision*, V1(4):321–331, 1988.

K. Kiesler, M. Gugatschka, E. Sorantin, and G. Friedrich. Laryngo-tracheal profile: A new method for assessing laryngo-tracheal stenoses. *European Archives of Oto-Rhino-Laryngology*, 264(3):251–256, 2007.

K. S. Lee and P. M. Boiselle. Tracheal and bronchial neoplasms. In P. M. Boiselle and D. Lynch, editors, *CT of the Airways*, pp. 151–190. Humana Press–Springer, New York, 2008.

K. S. Lee, W. Lunn, D. Feller-Kopman, A. Ernst, H. Hatabu, and P. M. Boiselle. Multislice CT evaluation of airway stents. *Journal of Thoracic Imaging*, 20(2):81–88, 2005.

P. Lee, E. Kupeli, and A. C. Mehta. Airway stents. *Clinics in Chest Medicine*, 31(1):141 –150, 2010.

M. Mandour, M. Remacle, P. van de Heyning, S. Elwany, A. Tantawy, and A. Gaafar. Chronic subglottic and tracheal stenosis: Endoscopic management vs. surgical reconstruction. *European Archives of Oto-Rhino-Laryngology*, 260(7):374–380, 2003.

R. A. McLaughlin, J. P. Williamson, M. J. Phillips, J. J. Armstrong, S. Becker, D. R. Hillman, P. R. Eastwood, and D. D. Sampson. Applying anatomical optical coherence tomography to quantitative 3d imaging of the lower airway. *Optics Express*, 16(22):17521–17529, 2008.

T. Miyazawa. History of the flexible bronchoscope. In B. C. T. and M. P. N., editors, *Interventional Bronchoscopy*, vol. 30, pp. 16–21. Karger, Basel, 2000.

T. Miyazawa, Y. Miyazu, Y. Iwamoto, A. Ishida, K. Kanoh, H. Sumiyoshi, M. Doi, and N. Kurimoto. Stenting at the flow-limiting segment in tracheobronchial stenosis due to lung cancer. *American Journal of Respiratory and Critical Care Medicine*, 169(10):1096–1102, 2004.

B. Mostafa. Endoluminal stenting for tracheal stenosis. *European Archives of Oto-Rhino-Laryngology*, 260(9):465–468, 2003.

S. A. R. Nouraei, D. W. McPartlin, S. M. Nouraei, A. Patel, C. Ferguson, D. J. Howard, and G. S. Sandhu. Objective sizing of upper airway stenosis: A quantitative endoscopic approach. *Laryngoscope*, 116(1):12–17, 2006.

K. Palágyi and A. Kuba. A 3d 6-subiteration thinning algorithm for extracting medial lines. *Pattern Recognition Letters*, 19:613–627, 1998.

P. K. Parida and A. K. Gupta. Role of spiral computed tomography with 3-dimensional reconstruction in cases with laryngeal stenosis–a radioclinical correlation. *American Journal of Otolaryngology*, 29(5):305–311, 2008.

R. Pinho, S. Luyckx, and J. Sijbers. Robust region growing based intrathoracic airway tree segmentation. *2nd International Workshop on Pulmonary Image Analysis*, pp. 261–271, London, September 2009.

U. B. S. Prakash. Advances in bronchoscopic procedures. *Chest*, 116(5):1403–1408, 1999.

M. Prasad, J. P. Bent, R. F. Ward, and M. M. April. Endoscopically placed nitinol stents for pediatric tracheal obstruction. *International Journal of Pediatric Otorhinolaryngology*, 66(2):155–160, 2002.

Y. Saito and H. Imamura. Airway stenting. *Surgery Today*, 35(4):265–270, 2005.

D. Shitrit, P. Valdsislav, A. Grubstein, D. Bendayan, M. Cohen, and M. Kramer. Accuracy of virtual bronchoscopy for grading tracheobronchial stenosis: Correlation with pulmonary function test and fiberoptic bronchoscopy. *Chest*, 128(5):3545–3550, 2005.

E. Sorantin, C. Halmai, B. Erdôhelyi, K. Palágyi, L. Nyúl, L. K. Ollé, B. Geiger, F. Lindbichler, G. Friedrich, and K. Kiesler. Spiral-CT–based assessment of tracheal stenoses using 3-D skeletonization. *IEEE Transactions on Medical Imaging*, 21(3):263–273, 2002.

E. Sorantin, D. Mohadjer, L. Nyúl, K. Palágyi, F. Lindbichler, and B. Geiger. New advances for imaging of laryngotracheal stenosis by post processing of spiral-CT data. In W. Hruby, editor, *Digital (R)Evolution in Radiology—Bridging the Future of Health Care*, pp. 297–308. Springer, New York, 2006.

N. Spittle and A. McCluskey. Lesson of the week: Tracheal stenosis after intubation. *British Medical Journal*, 321(7267):1000–1002, 2000.

S. Stamenkovic, R. Hierner, P. De Leyn, and P. Delaere. Long-segment tracheal stenosis treated with vascularized mucosa and short-term stenting. *Annals of Thoracic Surgery*, 83(3):1213–1215, 2007.

J. Stephens, Kenton E. and D. E. Wood. Bronchoscopic management of central airway obstruction. *Journal of Thoracic and Cardiovascular Surgery*, 119(2):289–296, 2000.

J.-M. Triglia, S. Marciano, B. Nazarian, G. Moulin, I. Sudre-Levillain, and A. Giovanni. Virtual laryngotracheal endoscopy based on geometric surface modeling using spiral computed tomography data. *Annals of Otology, Rhinology and Laryngology*, 111(1):36–43, 2002.

J. K. Udupa and S. Samarasekera. Fuzzy connectedness and object definition: Theory, algorithms, and applications in image segmentation. *Graphical Models and Image Processing*, 58 (3):246–261, 1996.

R. Valdés-Cristerna and O. Yáñez-Suárez. Active contours and surfaces with cubic splines for semiautomatic tracheal segmentation. *Journal of Electronic Imaging*, 12(1):81–96, 2003.

R. Valdés-Cristerna, O. Yáñez-Suárez, and V. Medina. Trachea segmentation in CT images using active contours. *Engineering in Medicine and Biology Society, 2000. Proceedings of the 22nd Annual International Conference of the IEEE*, vol. 4, pp. 3184–3187, 2000.

F. Venuta, E. A. Rendina, and T. de Giacomo. Airway stenting. Available at http://www.ctsnet.org/sections/clinicalresources/thoracic/expert_tech-1.html (accessed Nov. 2004).

E. M. Webb, B. M. Elicker, and W. R. Webb. Using CT to diagnose nonneoplastic tracheal abnormalities: Appearance of the tracheal wall. *American Journal of Roentgenology*, 174 (5):1315–1321, 2000.

J. P. Williamson, J. J. Armstrong, R. A. McLaughlin, P. B. Noble, A. R. West, S. Becker, A. Curatolo, W. J. Noffsinger, H. W. Mitchell, M. J. Phillips, D. D. Sampson, D. R. Hillman, and P. R. Eastwood. Measuring airway dimensions during bronchoscopy using anatomical optical coherence tomography. *European Respiration Journal*, 35(1):34–41, 2010.

D. E. Wood, Y.-H. Liu, E. Vallieres, R. Karmy-Jones, and M. S. Mulligan. Airway stenting for malignant and benign tracheobronchial stenosis. *Annals of Thoracic Surgery*, 76(1):167–174, 2003.

X. Xie and M. Mirmehdi. MAC: Magnetostatic active contour model. *IEEE Transactions on Pattern Analysis and Machine Intelligence*, 30(4):632–646, 2008.

C. Xu and J. Prince. Snakes, shapes, and gradient vector flow. *IEEE Transactions on Image Processing*, 7(3):359–369, 1998.